Final Technical Report

Discovering the Role of Grain Boundary Complexions in Materials

Award #: DE-FG02-08ER46548

Submitted by
Prof. Martin P. Harmer
Center for Advanced Materials and Nanotechnology
Lehigh University
5 E. Packer Avenue, Whitaker Laboratory
Phone: 610 7584227
Fax: 610 7583526
E-mail: mph2@lehigh.edu

Submitted to
Dr. Jane G. Zhu,
Program Manager
Electron and Scanning Probe Microscopies
Division of Materials Sciences and Engineering
Office of Basic Energy Sciences
U.S. Department of Energy
SC-22.2/Germantown Building
1000 Independence Avenue, SW
Washington, DC 20585-1290
Phone: (301) 903-3811
Fax: (301) 903-9513
E-mail: Jane.Zhu@science.doe.gov

Cheryl L. Howard, SC-22.2
Program Assistant
Office of Basic Energy Science
U.S. Department of Energy
Germantown Building
1000 Independence Avenue, SW
Washington, DC 20585-1290
Phone: (301) 903-3428
Fax: (301) 903-9515
E-mail: Cheryl.Howard@science.doe.gov

1. DOE award # and name of the recipient
DOE award #: DE-FG02-10ER46548
Recipient: Lehigh University

2. Project Title and name of the PI
Title: Discovering the Role of Grain Boundary Complexions in Materials
PI: Prof. Martin P. Harmer

3. Date of the report and period covered by the report
Date of the Report: March 19th, 2015
Period Covered: June 1st, 2009 to May 31st, 2011

4. A brief description of accomplishments.

Background

"*Complexion*" is a new classification scheme for grain boundaries, wherein grain boundaries are considered as phase like states of matter analogous to bulk thermodynamic phases in this new taxonomy. Numerous forms of grain boundary complexions can exist. The formation and stability of complexions are dictated by the thermodynamic variables such as temperature, stress (pressure), interfacial chemistry (chemical potential) and most importantly by the energies of the adjoining crystal surfaces. These grain boundary complexions are only stable within the constraint of the adjoining grains. Although complexions are not stable in bulk form, they can transform from one complexion to another as a function of various thermodynamic variables analogous to bulk phases. The presence of complexions and their transitions has been predicted by different computational thermodynamics approaches.

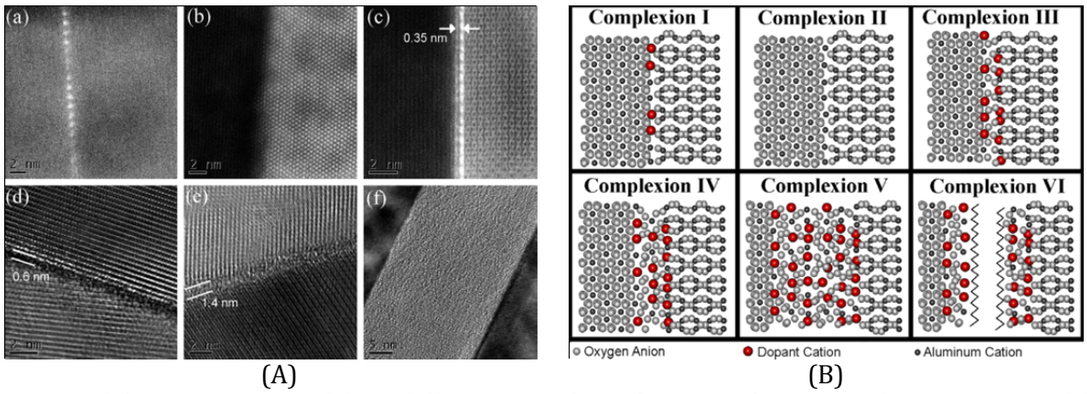

(A) (B)

Figure 1. (A) HREM images of the 6 different grain boundary complexions in alumina. Images (a) through (f) correspond to complexions I through VI respectively; (B) Schematic representation of the complexions.

In alumina (Al_2O_3) six distinctly different complexions have been observed with the aid of aberration corrected high resolution electron microscopy (HREM), as shown in Figure 1A. The complexions in these materials were stabilized by varying the chemistry (dopant material and concentration) and processing temperature. Each of these complexions has distinctly different grain boundary mobility. The complexions are numbered in order of increasing grain boundary mobilities. Long standing problems such as abnormal grain growth and chemically induced grain boundary embrittlement can be explained with this concept. Abnormal grain growth has been associated with the presence of two or more different coexisting complexions. The intergranular films that are observed in various ceramics and metals are just one of the complexions that can be present in those materials.

The goal of our current DOE-BES-funded research program was to verify the existence of grain boundary complexions in a range of materials systems, and to characterize their structures, range of stability, etc. The research program was a follow up of a breakthrough experimental study on the grain growth kinetics of alumina and atomic resolution electron microscopy of grain boundaries that revealed the presence of six different complexions in alumina-based materials. Materials systems studied include yttrium oxide, strontium titanate, silicon and titanium oxide. Each of these host materials represents a model material whose bulk properties are well established; for example, ytrrium oxide is a model transparent ceramic oxide with a stable cubic fluorite derived structure, and titanium oxide is a model electronic ceramic material. In the following sections, we summarize the results from these systems.

Grain Boundary Complexions in Si-Au

We undertook a study in the Si-Au system, in which Si bicrystals were made with a thin sputtered layer of Au in between the two Si crystals. Two orientations of bicrystals were studied: a (100) $\sum$29 boundary, and a (111) $\sum$43 boundary. We discovered distinctly different complexions in these two cases, with a disordered monolayer forming in the (100) $\sum$29 bicrystals, and an intrinsic ("clean") and Au-rich bilayer interfacial phase forming in the (111) $\sum$43 bicrystals.

The first study on (100) $\sum$29 boundaries was motivated by a recent atomistic simulation by Sutton and co-workers [1] that indicated that the Si (100) $\sum$29 grain boundary would undergo structural transitions starting at 0.7-0.8 T_m. Since Si-Au is one of the best metallic glass forming systems, we would expect that adding Au would promote the formation of "disordered" grain boundary structures. Surprisingly, our characterization showed that the Si (100) $\sum$29 grain boundaries in the Si-Au system only exhibited low levels of structural disorder with submonolayer adsorption of Au; in these experiments, we heated the specimens up to ~1 K below the melting temperature of Si (*i.e.*, > 0.999 T_m) and gas-quenched these specimens (where the initial cooling rate was as high as 500K/minute. Although we have done our best in quenching these specimens, we have to recognize that the observed grain boundary structures may have formed during the cooling. The most "disordered" grain boundary structure observed for all the (100) $\sum$29 grain boundaries that we have characterized is shown in Figure .

The second study on (111) $\sum$43 boundaries yielded the very interesting result that an intrinsic (clean) grain boundary complexions coexists along the same boundary as an Au-rich bilayer interfacial phase, with the transition between the two being abrupt. This abrupt transition suggests a first-order transition between these two interfacial phases. Figure 2 shows the entire series of grain boundary behavior observed in this bicrystal: (a) shows the withdrawing "tip" of the boundary, with Region B being an Au-rich bilayer complexion. In Region C, the bilayer becomes "intermittent", transitioning abruptly between "clean" and bilayer regions. We have very recently discovered that these intermittent bilayers are in fact continuous in the direction of the transmitted beam, and can be considered as Au "ultra-nanowires" as discussed below. Finally, Region D shows the intrinsic ("clean") grain boundary complexion. An interesting aspect of this result is that the monolayer complexion was totally absent: the bilayer transitioned directly and abruptly to an intrinsic ("clean") boundary. This transition presumably took place during cooling. Importantly, this study represents the first demonstration of the concept of "complexion-transitions" in a semiconductor system, suggesting that it is indeed a general phenomenon.

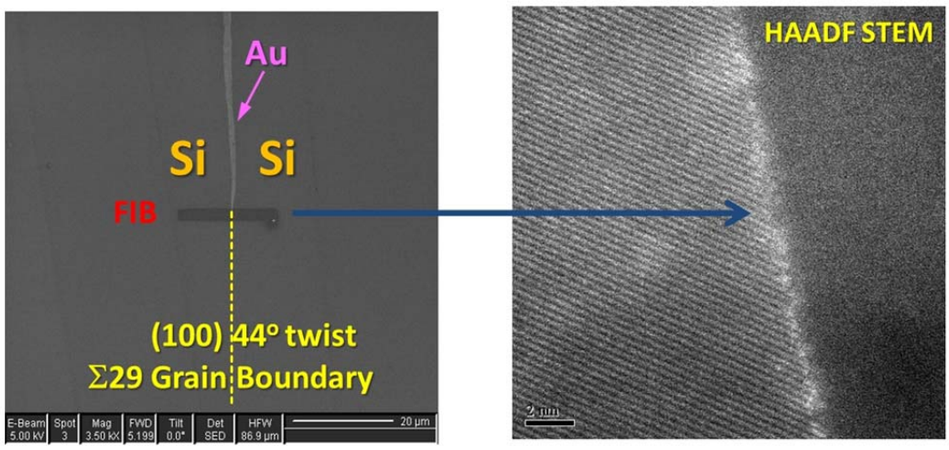

Figure 1: The most "disordered" (100) Σ29 grain boundary observed in this study.

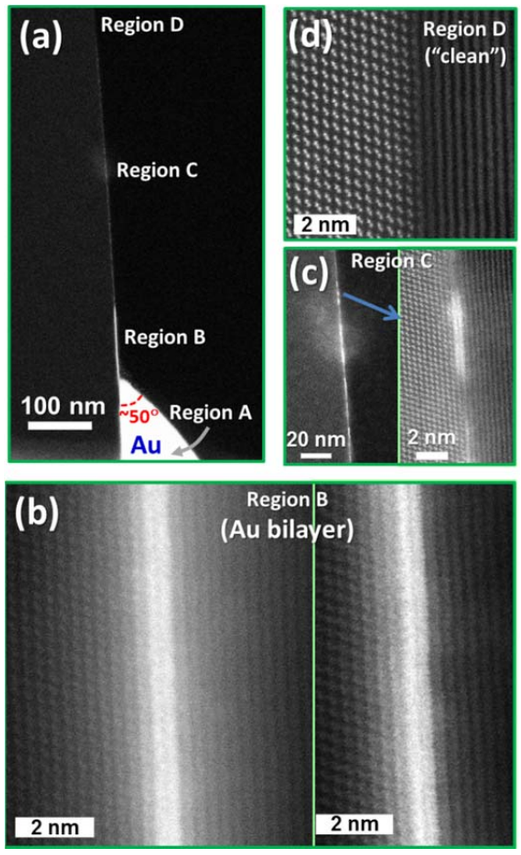

Figure 2: HAADF STEM micrographs of **(a)** a withdrawing Au drop at the interface of a Si bicrystal, which presumably formed during cooling. **(b)-(d)** are views of the Regions B, C and D, respectively, at higher magnifications. Reprinted from the DOE supported publication in Scripta Mater.

Our most recent observation, also in the Si (111) ∑43 twist grain boundary, has shown that Region C in Figure 2, which contains intermittent Au-rich bilayers separated by clean grain boundary, is actually a region of step-stabilized, bilayer-like, "ultra-nanowires" that are ~ 2-atoms

thick and 5 to 10 atoms wide. A series of HAADF-STEM images showing the Au bilayer ultra-nanowires is presented in Figure 3. This discovery was made during tilting experiments to verify that the bilayer is in fact a true bilayer (rather than a monolayer that appears to be a bilayer due to a through-thickness atomic step effect). When tilted to ~20 degrees, the "ultra-nanowires" are clearly visible, as shown in Figure (b) and (c). We believe that these Au nanowires are macroscopic in length. However, we are constrained to observing segments that are about 20 to 100 nm long due to TEM sample thickness limitations; the nanowires extend through the entire thickness of the TEM sample.

The Au nanowires have been observed in three different TEM samples collected from the same Si-Au bicrystal specimen via the in-situ FIB lift-out method. In all cases, the Au nanowires are about 2 atoms thick, 5 to 10 atoms wide, and extended through the entire TEM sample, suggesting that they are macroscopic in length. They are spaced periodically along the bicrystal boundary. However, the spacing between nanowires is different for each of the three TEM samples: 4 nm, 20 nm, and 55 nm. We believe that these differences in Au nanowire spacing are due to different bicrystal boundary plane orientations, i.e., the boundary plane orientation is not constant within the Si-Au bicrystal specimen and it is not perfectly parallel to the (111) planes in each Si crystal. The Au nanowire periodicities of 4 nm, 20 nm, and 55 nm suggest boundary plane tilts of 4.5°, 0.9°, and 0.3°, respectively, away from the (111) planes. This boundary plane misorientation results in atomic steps along the boundary where individual (111) crystal planes terminate. This causes the continuous region of the Au bilayer to "step" back and forth along the boundary as shown in Figure (f). The Au nanowires are positioned at these atomic steps where (111) planes terminate. Thus, the Au nanowires can be said to be both interface-stabilized and step-stabilized. We believe that this is the first report of a method to create subsurface nanowires.

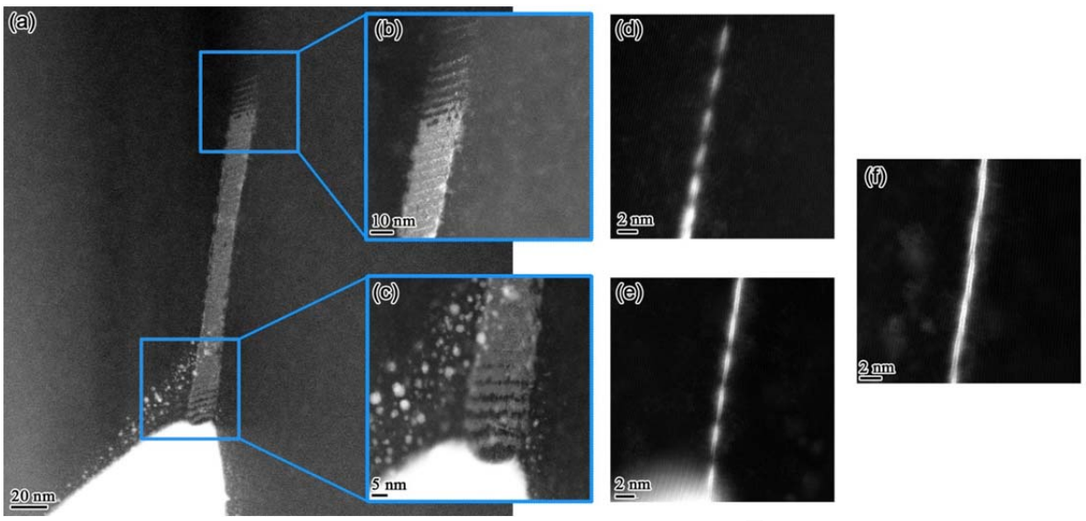

Figure 3: A bilayer of Au segregated to a Si (111) twist boundary (∑43). A large Au precipitate is visible at the bottom of (a). Figures (a)-(c) show the boundary tilted 20° away from the edge-on orientation so that the three-dimensional structure of the Au segregation at the boundary can be seen. Figures (d) and (e) show the edge-on view of the Au bilayer "nanowires" visible in (b) and (c), respectively; (f) shows the edge-on view of the continuous Au bilayer segment.

It is important that we briefly describe our efforts to minimize imaging artifacts when observing bilayer and trilayer interfacial phases (for this Si-Au study, as well as all other studies involving these structures). In S/TEM imaging, we must consider that we are viewing a two-dimensional projection of a three-dimensional object, and this raises the possibility of image misinterpretation. In our research, we always make a concerted effort to rule out such imaging artifacts, which are of particular concern for the bilayer and trilayer interfacial phases, such as the

Si-Au bilayer (Figure). In principle, it is possible for a monolayer to appear as a bilayer in a projected STEM image if there is a through-thickness atomic step, as shown schematically in Figure 4(a). The true bilayer structure in Figure 4(b) would also appear as a bilayer.

To discern between these two cases, we always obtain a series of through-focal images in which the incident electron probe is focused at different depths through the sample thickness. Two such values of defocus are shown in Figure 4, as Δf_1 and Δf_2. In the case of a bilayer, as in Figure 4(b), both sides of the bilayer will appear to be equally well focused throughout the entire focal series. For the case of a stepped monolayer, as in Figure 4(a), when one side of the apparent "bilayer" is in focus, the other side will not be. There is a defocus value in which both sides will appear to be equally in focus, which is why we obtain a focal series through the entire thickness of the TEM sample. A similar case arises when imaging a trilayer (not shown): both a monolayer and a bilayer, combined with the appropriate number of atomic steps through the sample thickness, could appear to be a trilayer in projection.

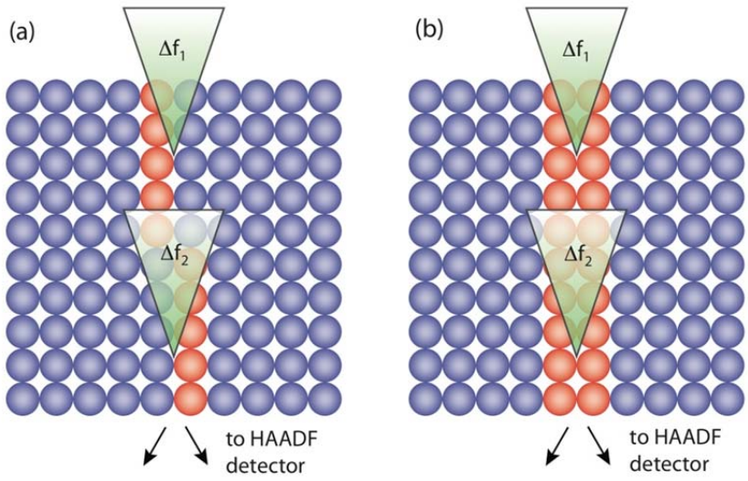

Figure 4: A schematic diagram showing (a) a monolayer that appears as a bilayer due to through-thickness atomic steps, and (b) a true bilayer. We discern between these two structures by obtaining a series of HAADF-STEM images at different values of defocus (e.g., Δf_1 and Δf_2). The electron probe is represented by the green triangles.

Grain Boundary Complexions in TiO_2-CuO

In this part of the research we investigated the grain boundary complexions in titania doped with various elements. We conducted initial screening experiments to determine specific dopants and annealing temperatures amenable to the formation of multiple complexions. The different dopants examined included oxides of boron, copper, zinc, silicon, yttrium and calcium. Preliminary results indicated a drastic increase in grain growth kinetics in copper oxide doped materials as compared to the undoped materials indicating the presence of multiple complexions. To elucidate the associated grain boundary complexions, several well-controlled model experiments have been conducted on undoped and CuO-doped rutile bicrystal sandwich samples. As shown schematically in Figure 5(a), a thin layer of CuO dopant was introduced in between two rutile single crystal substrates with known orientation (planar orientations of (100) and (001)) and hot-pressed in vacuum to form a diffusion bond at the interfaces. Subsequently the samples were annealed at 850 °C for 24 hours (which is below the eutectic temperature of 919 °C) and then air quenched. A phase diagram of the TiO_2-CuO system is shown in Figure 5(b).

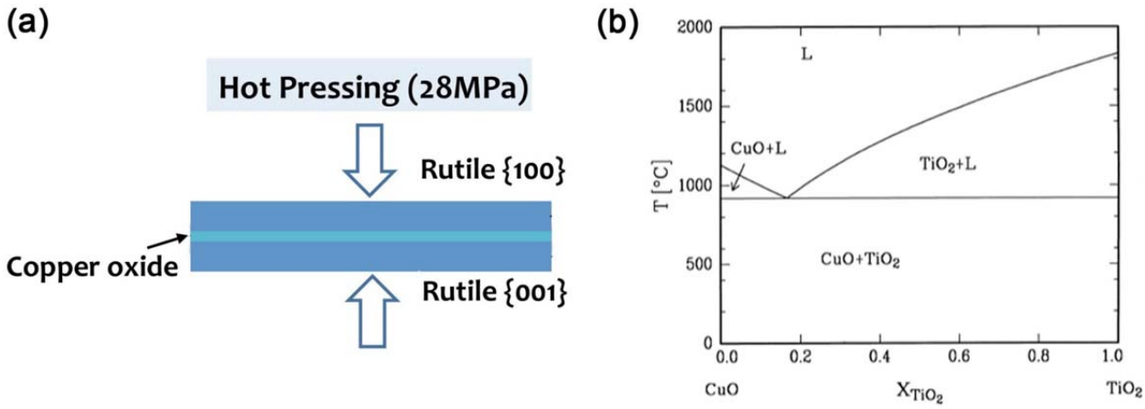

Figure 5: (a) Schematic of experimental setup showing hot pressing of bicrystals, including TiO_2 planar orientations; (b) phase diagram for TiO_2-CuO.

With the aid of HRTEM and aberration corrected high angle annular dark field-scanning transmission electron microscopy (HAADF-STEM) imaging, the coexistence of four distinct grain boundary phases was observed along the same rutile bicrystal grain boundary penetrated by copper oxide, as shown in Figure 6. An abrupt transition between these complexions was observed along the grain boundary in these samples. The sample was air quenched in the aforementioned experiments. We hypothesize that the cooling rate was not fast enough to preserve the high temperature complexion and that the boundary underwent several complexion transitions during cooling, which were kinetically trapped and preserved after cooling. The observed abrupt transitions from monolayer to bilayer, and from bilayer to trilayer, indicate that these grain boundary transitions are of first-order. This observation can be well explained with a premelting/prewetting type phenomenological thermodynamic model considering a structural oscillatory (solvation) interaction developed by the PI at Clemson University.

In collaboration with the STEM group at ORNL led by Dr. T. J. Pennycook, a detailed analysis of the nature of bonding at these grain boundaries was performed. To begin with, a nanoscale amorphous wetting film (complexion VI) ~ 5 nm thick was chosen for the analysis (Figure 7(a) and (b)). An EELS spectrum of this amorphous film and the adjacent grain in Figure 7 (c) indicates a significant intensity reduction of the Ti L edge at the grain boundary. Since the intensity changes observed for the corresponding O edge are much smaller (Figure 7 (c)) it was inferred that the reduction of the Ti edge intensity was not primarily due to thickness differences. Comparison of the simulated EELS signals for crystalline and amorphous rutile suggests that the mean signal was unchanged in the crystalline and amorphous areas, as shown in Figure 8. Hence, the observed reduction in Ti L shell signal was not due to different channeling conditions. Therefore, it was deduced that most of the titanium atoms at the grain boundary are replaced by copper atoms or other impurity atoms. The modified O-edge EELS fine structure observed at the grain boundary, as compared with the bulk grain (Figure 7(c)), indicates a lowering of the coordination number at the grain boundary.

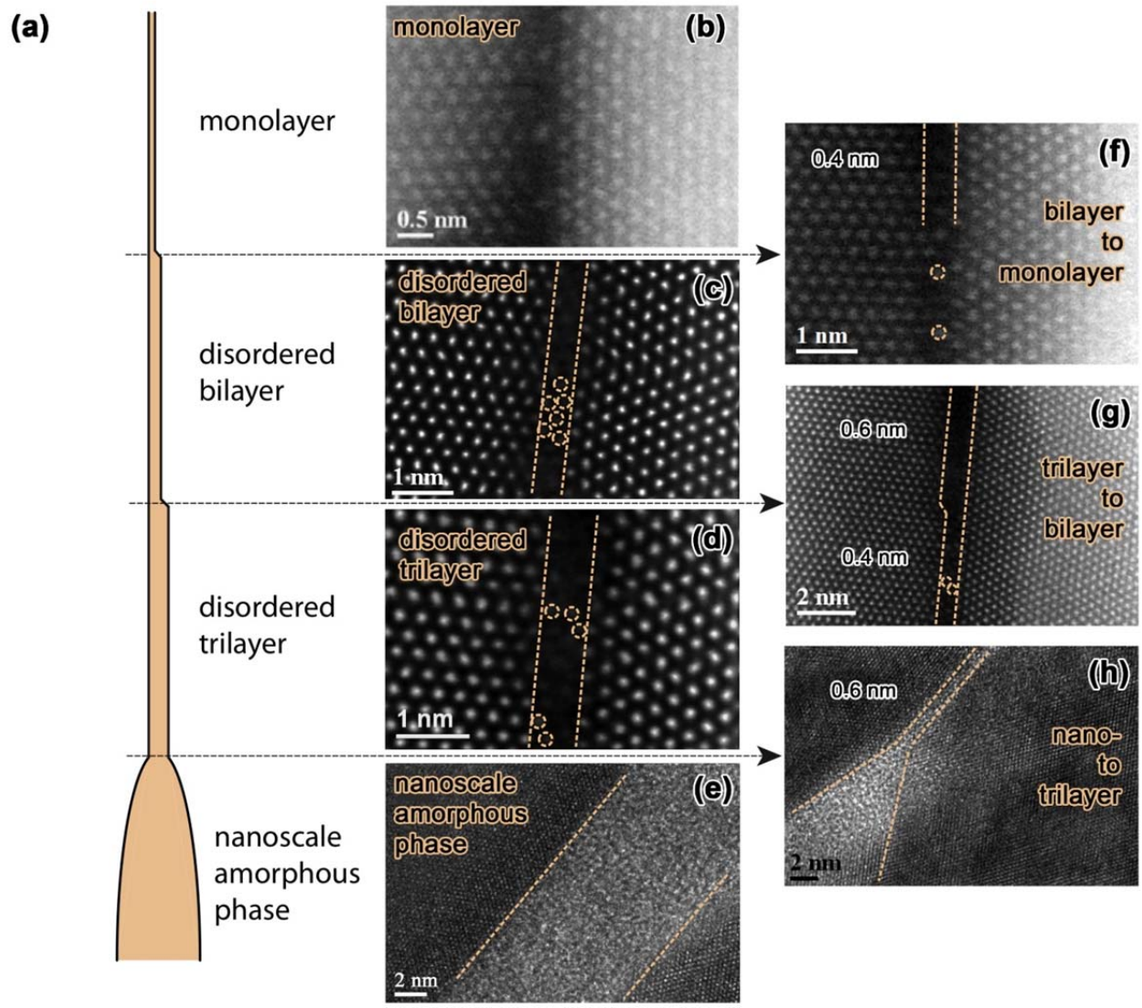

Figure 6: Interfacial phases observed at bicrystal boundary in the TiO_2-CuO system: (a) schematic diagram showing interfacial phase structure along bicrystal boundary; (b) – (e) STEM and HRTEM images showing monolayer, bilayer, trilayer, and amorphous nanoscale interfacial phases; (f) – (h) STEM and HRTEM images showing transitions between these interfacial phases, which are abrupt, suggesting first order behavior.

We point out that the contrast in the HAADF-STEM images of interfacial regions in Figure 6 (i.e., Figure 6(b), (c), (d), (f), (g)) is reversed from what we would expect for a Cu-rich interfacial phase. We believe that this contrast reversal is due to at least two effects: (1) the presence of SiO_2 and (2) the disordered nature of the interfacial phase. First, in a pure Z-contrast image, Cu (Z=29) would appear brighter than Ti (Z=22) while Si (Z=14) would be darker than both. Thus, the presence of SiO_2, which we have confirmed via EELS analysis, will tend to lower the brightness of this interfacial region. Second, the interfacial bilayer and trilayer phases are disordered, i.e., there are not ordered atomic columns extending directly through the sample, and therefore no strong electron channeling occurs. In the abutting crystalline grains, which are oriented on zone axis, electron channeling occurs and this has the effect of scattering more electrons into angles collected by the HAADF detector, making these regions appear brighter in the HAADF-STEM images. Several analogous examples exist in the literature demonstrating that amorphous

material may appear darker than crystalline material oriented on zone axis in annular dark field STEM images, e.g., as was demonstrated for a-Si versus c-Si [2].

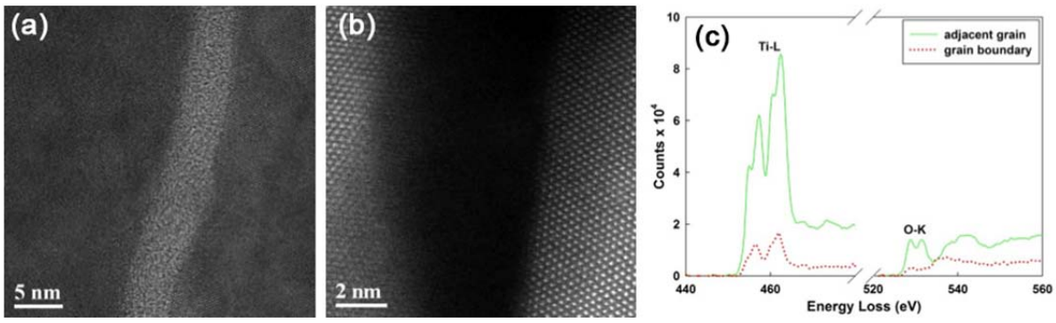

Figure 7: (a) BF-STEM and (b) HAADF-STEM images of a nanoscale amorphous film at the grain boundary in Fig. 1; (c) EELS spectra of the grain boundary and the adjacent grain, indicating a significant reduction of the Ti L peak intensity and a change of the O fine structure at the grain boundary.

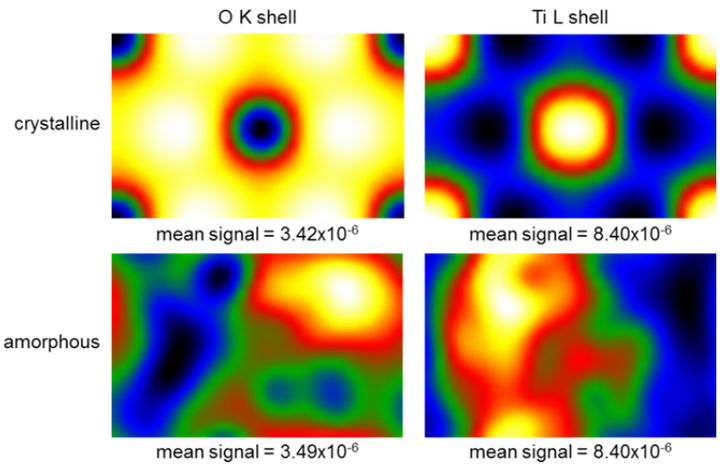

Figure 8: Comparison of the simulated EELS signals for crystalline and amorphous rutile, showing that the mean signal EELS intensity is invariant with degree of crystallinity. This confirms that the EELS spectra in **Figure** (c) do in fact demonstrate a reduction in Ti concentration at the grain boundary (rather than a variation in Ti L-edge intensity due to a crystalline channeling effect); hence, other impurity atoms (e.g., Cu, Si) must be present in the interfacial region in place of the Ti atoms.

Grain Boundary Complexions in Yttrium Oxide

The research on the yttrium oxide system was the first comprehensive study correlating the grain growth kinetics with the structure and chemistry of the grain boundaries in yttria. Several grain boundary complexions were observed in this material (Table 1). Surprisingly, the intrinsic impurities (such as silica and calcia) present in the powders rather than the added dopants (Yb/Er mixture) were discovered to be the principal contributor for the formation and stability of various complexions. The presence of silica suppressed grain growth in Y_2O_3 and stabilized a type I complexion (monolayer). Type II (clean boundaries) complexions were observed in the ultra-high purity undoped material. A small concentration of calcium (100 ppm) doping was found to be effective in promoting the grain growth kinetics in yttria. Type III or type IV complexions were

associated with the normal grain growth and type V for the abnormal grain growth in calcium-doped yttria. The annealing atmosphere was also found to affect the grain growth kinetics. The samples annealed in a reducing atmosphere (5% H_2 balanced N_2) had a higher activation energy for grain growth as compared to those annealed in an oxidizing atmosphere (air) as evident from the slope of the grain boundary mobility curves in Figure 9. The grain growth activation energies for ytrria samples annealed in air were in the range of 211 to 387 kJ/mol; for samples annealed in a reducing atmosphere it was within the range of 622 to 769 kJ/mol.

Table 1: Grain boundary complexions correlated with the grain growth behavior in various yttria samples annealed in 5%H_2-N_2.

Samples	**Grain Growth Behavior**	**Complexion Types**
500 ppm Si-doped Y_2O_3	suppressed grain growth	I
high-purity undoped Y_2O_3	intrinsic	II
100 ppm Ca-doped Y_2O_3	promoted normal grain growth	III or IV
100 ppm Ca-doped Y_2O_3	abnormal grains	V

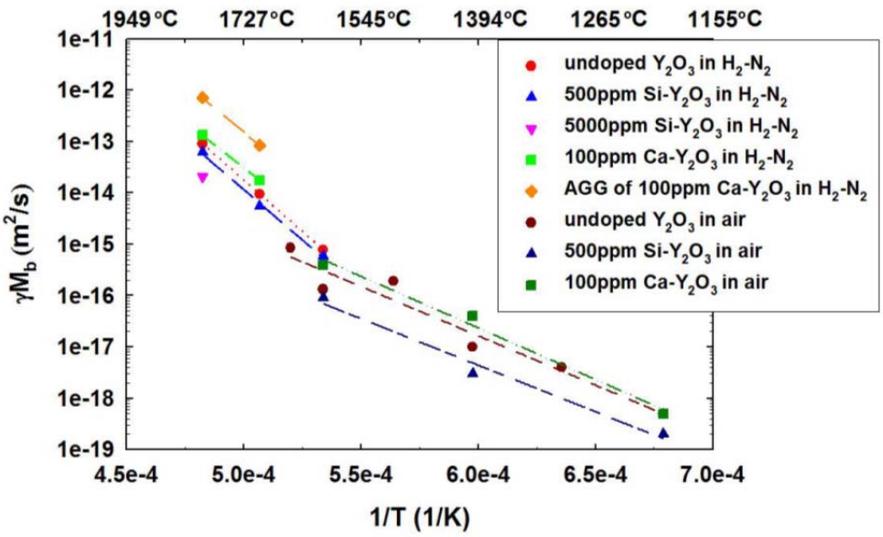

Figure 9: Grain boundary mobility for variously doped dense Y_2O_3 samples annealed in different atmospheres plotted as a function of temperature. The slope of the fitted curve is the activation energy for grain growth. Boundaries with distinctly different relative mobilities corresponded with different grain boundary complexions.

Grain Boundary Complexions in Strontium Titanate

In this work the effect of non-stochiometry (strontium- and titanium-rich compositions) on grain growth in strontium titanate was examined. This work was performed in collaboration with Prof. Michael J. Hoffmann's group at Institut für Keramik im Maschinenbau, Universität Karlsruhe and has been published in Acta Materialia. The fabrication and the grain growth kinetics of the samples were investigated at Universität Karlsruhe. Grain boundary chemistry was examined with

the aid of aberration corrected STEM-EDS at Lehigh University. Abnormal grains were observed in the temperature range from 1425°C to 1500°C in compositions with Sr/Ti ≤ 1.002. With Sr/Ti = 1.005 normal grain growth occurs with a grain boundary mobility that is associated with the mobility of the abnormal grain boundaries of the other compositions. The most interesting feature of this chemical analysis is that the local Sr/Ti-ratio cannot be directly correlated to the bulk composition (Figure 10). The material with a small strontium excess (Sr/Ti = 1.002) shows nearly the same frequency of titanium rich and neutral boundaries as the titanium-rich material (Sr/Ti = 0.996). Additionally, the boundary composition varies with temperature. These results indicate that grain boundaries provide additional degrees of freedom, making compositions possible at grain boundaries (that are not stable as a bulk phase) whose stability is dictated by the temperature just like bulk phases directly corroborating the grain boundary complexion theory. Also these results indicate that the grain boundary complexions are not merely impurity driven but can result from non-stoichiometry as well.

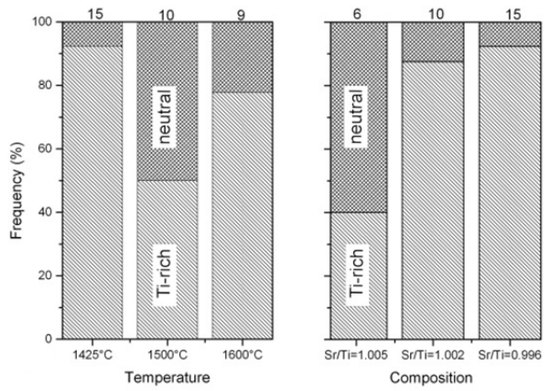

Figure 10: Frequencies of normal and Ti-rich boundaries. Number of measured boundaries is given in top row: a) Ti-rich material (Sr/Ti=0.996) annealed at different temperatures (1425°C for 20h, 1500°C for 4h and 1600°C for 0.5h), b) variation of Sr/Ti-ratio with constant annealing conditions (1425°C, 20h).

Publications

- S. Ma, P. R. Cantwell, T. J. Pennycook, N. Zhou, M. P. Oxley, D. N. Leonard, C. J. Kiely, S. J. Pennycook, J. Luo and M. P. Harmer, "Grain boundary complexion transitions in WO3- and CuO-doped TiO2 bicrystals," Acta Materialia, 61[5] 1691-1704 (2013).
- S. Ma, K. Meshinchi Asl, C. Tansarawiput, P.R. Cantwell, M. Qi, M. P. Harmer, and J. Luo, "A Grain Boundary Transition in Si-Au," Scripta Materialia, 66[5] 203-206 (2012).
- S. Ma and M. P. Harmer, "Near-Intrinsic Grain Boundary Mobility in Dense Yttria", J. Am. Ceram. Soc., 94 (2011) 651-5
- S. Ma, T. J. Pennycook, M. P. Oxley, D. N. Leonard, C. J. Kiely, S. J. Pennycook, and M. P. Harmer, "Grain Boundary Complexions in TiO_2 Bicrystals Doped with CuO," Microscopy and Microanalysis, in press (2011).
- M. P. Harmer, "The Phase Behavior of Interfaces," Science, 332 (2011) 182
- M. Bäurer, S.-J. Shihb, C. Bishop, M. P. Harmer, D. Cockayne and M. J. Hoffmann, "Abnormal Grain Growth in Undoped Strontium and Barium Titanate," Acta Materialia, 58[1] 290-300 (2010).
- M. P. Harmer, "Interfacial Kinetic Engineering: How Far Have We Come since Kingery's Inaugural Sosman Address?" Journal of the American Ceramic Society, 93 [2] 301-317 (2010).

- S. J. Dillon, M. P. Harmer, and J. Luo, “Grain Boundary Complexions in Ceramics and Metals: An Overview” (invited), JOM, 61 [12], 38-44 (December 2009).
- J. Luo, S. J. Dillon and M.P. Harmer, “Interface-Stabilized Nanoscale Quasi-Liquid Films” (overview article for non-specialists), Microscopy Today, 17 [4], 22-26, July 2009.

References Cited

[1] von Alfthan S, Kaski K, Sutton AP. Molecular dynamics simulations of temperature-induced structural transitions at twist boundaries in silicon. Phys. Rev. B 2007;76:245317.
[2] Yu Z, Muller DA, Silcox J. Relative contrast in a-Si and c-Si in ADF-STEM imaging. Microsc. Microanal. 2003;9:848.